ACS APPLIED MATERIALS & INTERFACES

Research Article

www.acsami.org

Atomic Layer Deposition of Metal Oxide Patterns on Nonwoven Fiber Mats using Localized Physical Compression

William J. Sweet, III, Christopher J. Oldham, and Gregory N. Parsons*

Department of Chemical and Biomolecular Engineering, North Carolina State University, Raleigh, North Carolina 27695, United States

ABSTRACT: Patterning is an essential part of many industrial processes from printing to semiconductor manufacturing. In this work, we demonstrate a new method to pattern and selectively coat nonwoven textiles by atomic layer deposition (ALD) using compressive mask patterning. A physical mask combined with mechanical compression allows lateral definition and fidelity of the ALD coating to be controlled. We produce features of several sizes on different nonwoven fiber materials and demonstrate the ability to limit diffusion effects to within <200 μm of the pattern edge. Lateral and vertical penetration of reactive growth species into nonwoven mats is investigated by plan-view and cross-sectional imaging. Vertical growth is also analyzed by imaging coating depth into fiber mat stacks. We develop a fully quantitative transport model that describes well the effect of fiber structure and mechanical compression on the extent of coating under the physical mask. This method could be implemented for high-volume patterning for applications including flexible electronics.

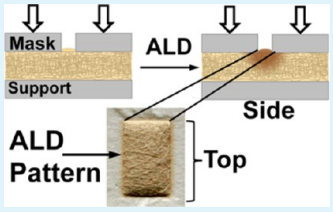

KEYWORDS: *patterning, atomic layer deposition, nonwoven, zinc oxide, flexible electronics*

INTRODUCTION

Patterning of thin films is a primary process in manufacturing of integrated circuits for electronic memory, logic, displays, and other systems.[1,2] There is growing interest in additive patterning processes where film patterns are formed directly on a substrate using substrate-selective reactions, chemical blocking layers, or surface-localized balancing of deposition/etch rates.[3] Shadow mask patterning is an early example of an additive process that takes advantage of line-of-sight species adsorption and reaction in thin film sputtering or other physical deposition processes.[4] When using shadow masks with more conformal deposition methods, including chemical vapor deposition (CVD), plasma CVD, and especially atomic layer deposition (ALD), precursor diffusion leads to film growth under the edge of the mask, making it difficult to generate well-defined patterns. For example, Langston et al.[2] found that for shadow-mask patterning during ALD onto planar silicon, the gap between the substrate and mask must be held near ~10 nm to achieve reliable patterning. Other studies of ALD growth profiles in pores or narrow slits[5,6] give insight into species diffusion and growth mechanisms during thermal or plasma-enhanced ALD.

Flexible, breathable, or stretchable substrate materials, including fibrous textiles and nonwoven fiber mats, have been explored as supports for unique integrated electronic device systems.[7,8] Fibrous substrates are readily available at low cost, and they are also interesting as substrate materials, in part, because of their physical dimension and aspect ratio (i.e. small diameter and long length). Under bending stress, the fiber shape helps to balance the mechanical forces encountered by thin conformal coatings, including forces that direct stress toward the coating/fiber interface. Weaving and surface printing technologies are well developed for fibrous media and studies have applied these approaches to integrate metal wires and other electronic elements.[7] However, electronic weaving or printing requires or produces relatively large wires, which add bulk and noticeably degrade the texture or "feel" of the fabric. There is growing interest in electronic "decals" that are affixed to finished products, but those also add bulk and diminish breathability.

Recently, researchers have explored vapor-phase atomic layer deposition and related methods to produce conformal metal and semiconductor thin film coatings on textiles and nonwoven fiber mats.[8−13] Atomic layer deposition enables conformal nanoscale metal coatings on fibers, for example, so that each fiber within a textile or nonwoven mat receives the same film layer thickness.[11−13] Nonwovens are interesting because they are made at very low cost and high rate and are used in many commercial, consumer, and engineered devices, ranging from personal hygiene products to high performance filtration devices and charge storage batteries. Coated fiber mats may provide a unique capacity for integrating electronic insulators, semiconductors, and metallic conducting layers onto nonwovens.[11−13] Because the coating is very thin (less than 100 nm)[11−13] the coating can remain intact and stay conductive, for example, without significantly affecting the fiber weight, flexibility, breathability, or tactile texture. However, results to date for metal ALD on fabrics are limited to coatings that cover the entire substrate surface. Electronic device integration into textiles is emerging and is interesting for large-area applications, such as temperature, gas, or liquid sensors, or for antennas or other communication elements. Patterning will be important

Received: March 19, 2014
Accepted: May 21, 2014
Published: May 21, 2014

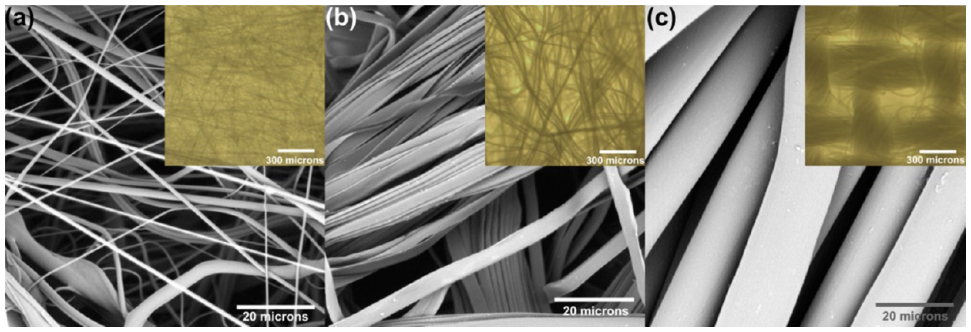

Figure 1. Scanning electron microscope (SEM) images of (a) polypropylene nonwoven, (b) nylon-6 nonwoven, and (c) nylon woven mats used in this study; all SEM scale bars are 20 micrometers. Insets are low magnification optical microscopy images of the respective substrates to show context for the SEM images; the scale bars for the inset images are 300 micrometers. Optical images are of the fibers as received; a 5 nm Au/Pd coating was sputtered onto the substrates prior to the SEM images.

for active layers, contacts, passivation, or other functional regions. Cost and simplicity will be critical, and because of the large substrate area, very large device feature sizes (0.1−1 mm or even larger) could be sufficient or even preferred. Early device applications could include integrated antennas and patterned electrodes or wiring in fiber-based electronics. Mask patterning is simpler and less costly than lithography. Large feature sizes could be sufficient for these uses, and approaches to minimize lateral species transport may enable smaller feature definition.

In this work, we demonstrate that compressive diffusion mask patterning applied to a porous fibrous mat substrate is a functional method to create metal oxide thin film patterns, with pattern control in both lateral and vertical directions on the substrate. To generate the pattern, a metal patterned mask is placed on top of a fiber mat, and the fibers beneath the covered regions are mechanically compressed, effectively restricting lateral precursor transport. The exposed area remains more open, allowing precursors and reactants to diffuse and deposit on surfaces throughout the region. In some instances, by controlling the time per ALD cycle that reactant species can diffuse vertically into the patterned zone, we also achieve a vertical pattern in the deposited film coating. In addition, we show that the characteristic structure and arrangement of the fibers in the fabric affect species diffusion and transport, and thereby, affect the pattern integrity and resolution.

EXPERIMENTAL SECTION

Fiber Substrate Materials. Images of nonwoven fiber mats and woven fiber fabrics used in this study are shown in Figure 1. Nonwoven melt-blown polypropylene (PP) was acquired from the Nonwovens Institute at the North Carolina State University with a basis weight of ∼39 g/m^2 and an as-received mat thickness of ∼0.3 mm (uncompressed).[14] Fibers within the mats had a circular cross-section with diameter in the 1−5 micrometer range. Samples were cut from the as-received nonwoven rolls into ∼2 cm × 3 cm pieces.[12] In addition, hydro-entangled nylon-6 (PA6) nonwoven Winged Fibers mats were acquired from Allasso Industries. The mats were approximately 0.4 mm thick (uncompressed) with a weight of ∼66 g/m^2. Individual fibers were 5−10 micrometers in diameter. The individual fibers had a lobed cross section[13] to increase the overall surface area.

To understand the extent of film growth on the fiber mats, we also analyze the total surface area of the fibers per unit area of fiber mat. This surface area enhancement factor, f_{SA} is a unitless value corresponding to the total fiber surface area per unit projected area of the fiber mat sample. The value for f_{SA} is determined by measuring the specific surface area of a nonwoven (m^2/g) using Brunauer−Emmett−Teller (BET) surface area analysis, followed by multiplying surface area by the sample basis weight (g/m^2) measured with a laboratory scale. For the polypropylene, we find f_{SA} = 1.6 m^2/g × 39 g/m^2 = 62, whereas for the nylon-6, f_{SA} = 2.5 m^2/g × 66 g/m^2 = 166.

Another important factor in the fiber materials is the overall void fraction, ε, that is, the fraction of space not occupied by solid polymer, and is found using the net fiber mat density ρ_m and the polymer density ρ_p. The fiber mat density is estimated from the fiber mat thickness t_m (which changes upon compression) and basis weight m_m

$$\rho_m = m_m/t_m \quad (1)$$

$$\varepsilon = 1 - \rho_m/\rho_p = 1 - m_m/(\rho_p \cdot t_m) \quad (2)$$

Using ρ_p = 0.99 g/cm^3 for polypropylene and 1.084 g/cm^3 for nylon-6, we obtain ε = 77% for partially compressed nylon-6, 53% for fully compressed nylon-6, 84% for partially compressed polypropylene, and 57% for fully compressed polypropylene.

During nonwovens fabrication, spun fibers are collected on a belt moving in the "machine direction" (MD), perpendicular to the "cross direction" (CD). Fiber orientation is generally random, but depending on the belt speed and fiber spinning output, the fibers in the nonwoven can take on a preferential orientation in the MD. Fiber imaging and analysis software in the Nonwovens Institute was used to determine the preferential orientation of the mats used for this study. The nylon mats showed some orientation in the machine direction, with 12% greater orientation in the machine direction and 10% less orientation in the cross direction than would be expected from a uniform distribution. By comparison, the melt-blown polypropylene is ∼6% preferentially oriented in the machine direction. Results for ALD on the nylon-6 show different extent of reactant diffusion in the MD and CD, as expected for partially aligned fibers. The diffusion appears uniform in direction for the polypropylene, consistent with a random fiber orientation. In this work, a "MD sample" has fibers oriented *perpendicular* to feature being patterned, whereas a "CD sample" has fibers oriented parallel to the feature direction.

Woven nylon fabric with a plain weave structure (∼125 g/m^2) was acquired from the NC State University College of Textiles. The weave consisted of fiber strands or yarns ∼250 micrometers in diameter, made up of many twisted fibers, each ∼15 micrometers in diameter. The fabric weave, composed of perpendicular warp and weft yarns, orients the fibers and creates a spatial variation in fiber density across the substrate. The yarn size, density, and type of weave strongly influence fluid and particle transport through the fabric.

Atomic Layer Deposition and Fiber Imaging. Atomic layer deposition of ZnO was performed in a homemade tubular hot-wall reactor described previously.[14] During processing, nitrogen carrier gas (99.999% N_2, National Welders) was filter dried (Aeronex Gatekeeper) and directed to flow continuously into the reactor at a flow rate of 150 standard cubic centimeters per minute (sccm). Pressure during deposition was typically ∼1.0 Torr, and temperature was fixed between 125 and 155 °C. Zinc oxide deposition was performed using

diethyl zinc (DEZ 95%, Strem Chemical) and water (UV-deionized, DI). The precursor and reactant dose times during ZnO ALD were typically fixed at $DEZ/N_2/H_2O/N_2$ = 2/40/2/40 seconds, respectively. The reactor pressure increased $\Delta P \approx 0.07$ Torr during precursor exposure and $\Delta P \approx 0.28$ Torr during the water exposure step.

For 400 ALD cycles at 125−155 °C, the ZnO ALD on the polypropylene and nylon-6 led to a distinct color change,[12] as shown for ZnO on polypropylene in Figure 2. Films deposited on glass slides

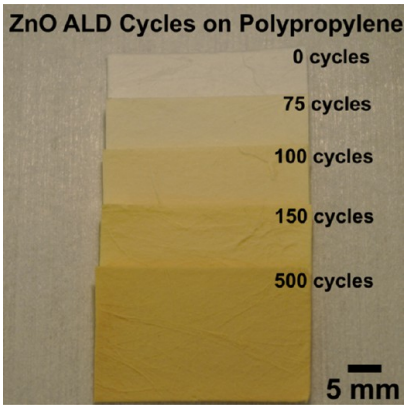

Figure 2. ZnO ALD on nonwoven polypropylene deposited at 155 °C, with different numbers of ALD cycles. The color change reflects the thickness of the ALD coating.

and quartz fibers also show similar coloration. The composition of the pattern was confirmed for several samples using energy dispersive X-ray spectroscopy (EDS) analysis of coated and uncoated regions. We find that 100 cycles of ZnO is not visibly distinct from uncoated nylon-6, whereas 200 cycles shows clear color change. When measuring the extent of coating, we maintain at least 400 ALD cycles, and visible imaging can therefore be used to compare patterns made under different processing conditions.

Optical images were collected using a high resolution digital SLR camera with macro-filter attachments for close up shots of the substrates. For some of these inset images, contrast was enhanced using GIMP 2.8 Graphics Software, as noted in the respective figure captions. High magnification optical images were taken using a Jenoptik optical microscope with a ProgRes CT5 digital microscope camera attachment. Microscope images were analyzed using ProgRes CapturePro 2.6 software package. For diffusion length measurements, for each data point at least two different samples were measured, in at least four different locations, for no less than eight measurements per data point. The measurements were taken from the same locations for all samples to maintain consistency.

Pattern Deposition and Processing. Patterning was performed by compressing the nonwoven or woven fiber samples between a pair of aluminum metal masking plates as shown schematically in Figure 3. The open areas on masking plates, which permitted precursors to diffuse into the fiber mats, could be on one or both of the plates, depending on the desired pattern.

The extent of compression was controlled by screws that held the plates together. The screws were finger-tightened and the plate separation was measured using a digital caliper; additional tightening was performed as required using a hex wrench. Two different values of compression were studied. The fibers were either "fully" compressed, where the plate spacing at 0.13 ± 0.02 mm for the nylon-6 nonwoven and 0.09 ± 0.02 mm for polypropylene nonwoven. For the "partially" compressed samples, the screws were tightened to provide a spacing of 0.25 ± 0.02 mm for polypropylene nonwoven and 0.27 ± 0.02 mm for the nylon-6 nonwoven samples. Unless otherwise stated, we used "fully" compressed samples for the studies described here.

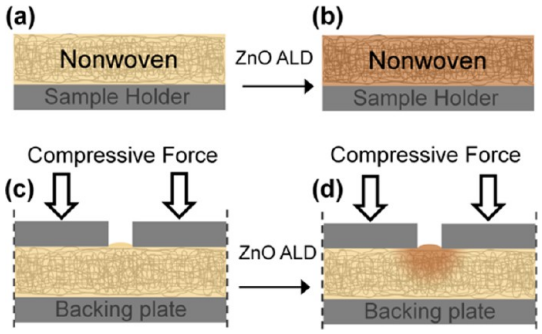

Figure 3. Schematic cross-section showing ALD coating on a nonwoven mat (a, b) without a mask and (c, d) with a compression mask in place. The mask limits lateral diffusion of the precursors within the nonwoven, producing a pattern that is restricted to exposed portions of the mask. This example shows a solid backing plate. The solid plate allows the extent of growth in the vertical direction to also be controlled by adjusting the precursor dose time per cycle.

RESULTS AND DISCUSSION

Figure 4a shows a sample mask with 10 mm wide slits, with lengths of 1.6, 3.2, 6.4, and 12.7 mm, spaced at least 5 mm apart

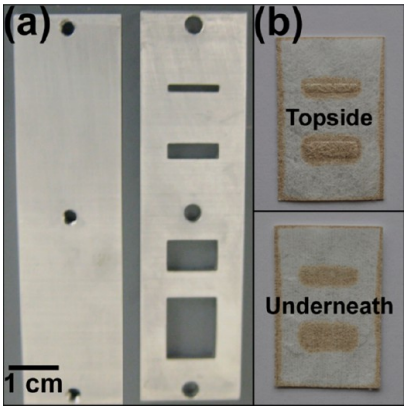

Figure 4. (a) Aluminum solid back plate and pattern mask with slits 10 mm wide and lengths of 1.6, 3.2, 6.4, and 12.7 mm, spaced at least 5 mm apart and 5 mm from the edge. (b) Both sides of a nylon-6 nonwoven patterned with 400 cycles of ALD ZnO at 155 °C show a pattern, demonstrating that the precursors vertically permeate through the nonwoven to also produce a pattern on the side that was covered by the solid metal back plate. The patterned color of the oxide is visible, with some coating also on the edge of the samples.

and 5 mm from the edge. Figure 4b shows the resulting pattern of ALD ZnO deposited using 400 cycles at 155 °C on the top and bottom sides of a MD nylon-6 substrate. The mask effectively limits precursor access only to the uncovered regions. The edges of the mat are also exposed, allowing visible growth around the sample border.

To verify the color change is due to the coating of ZnO ALD on the nonwoven, elemental analysis was performed by EDS on a ZnO patterned polypropylene substrate. Figure 5a shows a SEM image of the ZnO patterned polypropylene substrate along with EDS scans that were taken, the locations of which are indicated on the SEM image with corresponding numbers.

Inside the patterned region, the EDS results in Figure 5a,I show strong Zn and a relatively weak C signals, consistent with the patterned ZnO coating on polymer. In the transition region, which is the area that is compressed and located near the

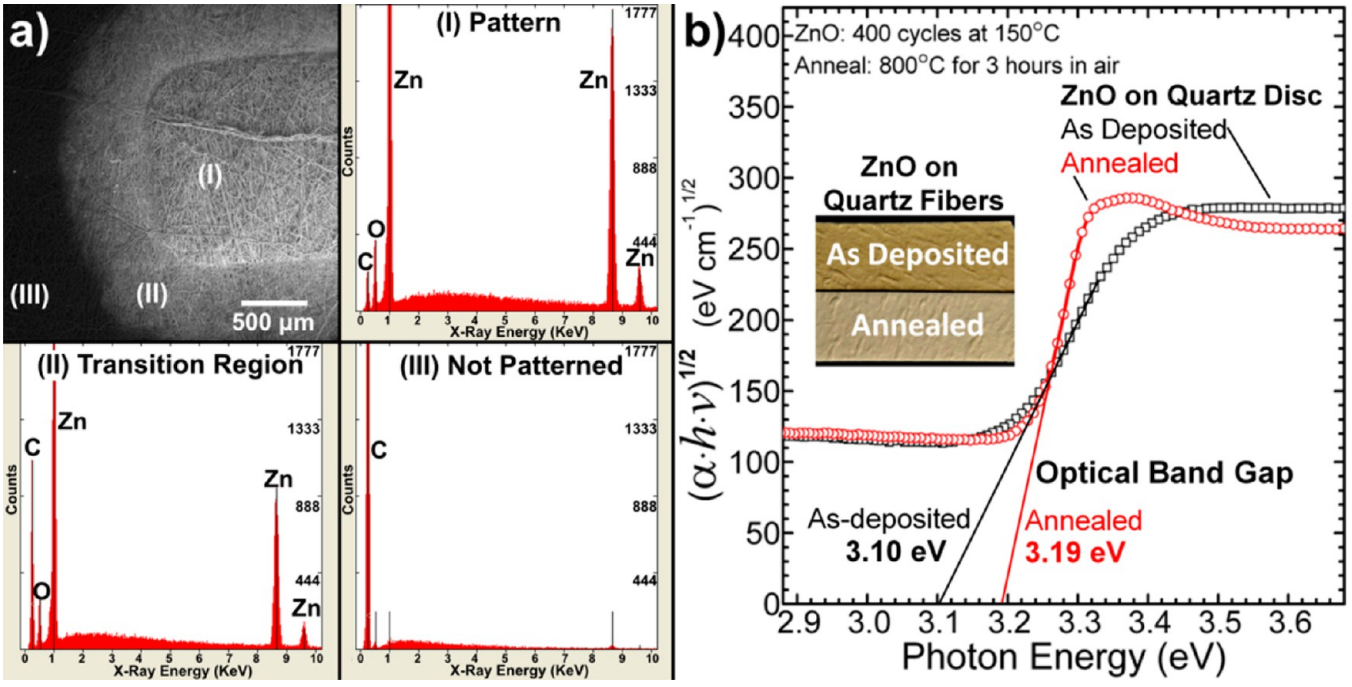

Figure 5. (a) SEM image and EDS scans of a ZnO patterned feature on a polypropylene nonwoven. The numbers on the image correspond to locations where the EDS scans were taken. (I) The patterned region is not covered by the mask. (II) The compressed region near the opening where DEZ diffuses during dosing. (III) Compressed region beyond where DEZ diffuses. The zinc signal is strongest relative to carbon in the patterned feature, location (I). Carbon signal is strongest in the region that is not patterned, and no zinc signal is detected. (b) Optical absorption data vs. photon energy for ZnO (400 cycles at 155 °C) on quartz discs, for as-deposited and after annealing at 800 °C in air for 3 h. Inset shows the same films deposited on quartz fibers. The visible color on the as-deposited fibers is ascribed to ZnO with oxygen vacancy or other related defects.

pattern opening, there is still a strong zinc peak but also a more significant carbon peak. In the uncoated region, the compressed area beyond where the DEZ could diffuse, EDS shows only carbon, with zinc below the detection limit. The zinc signals correspond well with the visible coloration of the sample, so the optical color can be used to identify the distance that the ZnO coating has progressed from the feature edge.

The red-brown color of our as-deposited ZnO is ascribed to oxygen vacancy or other related gap states in the films deposited at low temperature.[15,16] To confirm this, quartz discs were coated with 400 cycles of ZnO ALD at 155 °C for UV−vis analysis, and results for as-deposited and annealed (3 h at 800 °C in air) films are shown in Figure 5b. Upon annealing, the ZnO band gap increases from 3.10 to 3.19 eV, consistent with defect oxidation. Previous research[16] has shown as-grown ZnO single crystals with zinc rich stoichiometry are colored, and become visibly transparent upon high temperature anneal in air due to defect oxidation. We also find that white nonwoven quartz fiber mats coated with 400 ZnO ALD cycles at 155°C appear red-brown, and become more white colored upon 800°C anneal (inset, Figure 5b), again consistent with oxidation. The red-brown color on the fibers is therefore a good visible marker for extent of ZnO ALD.

To determine the extent of precursor diffusion, we use optical microscopy as shown in Figure 6. The growth extension under the mask is the distance between the mask edge (which is clearly visible in reflection mode) and the edge of the coating coloration (which is clearly visible in transmission mode).

The bottom panels in Figure 6 show an arrow, set by eye that corresponds to the measured distance for lateral growth under the mask. Using the magnification scale, we see that the ZnO coats approximately 1.25 mm into the polypropylene and 0.95

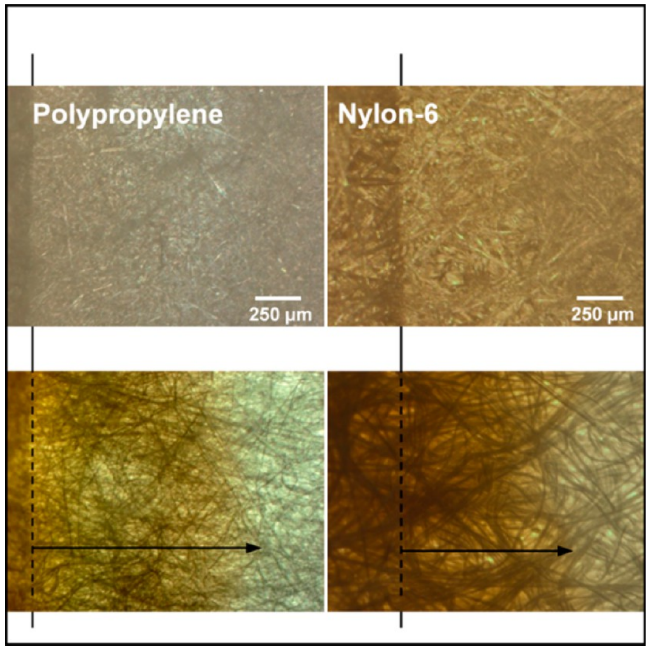

Figure 6. Optical microcopy in reflection (top images) and transmission mode (bottom) of patterned ZnO ALD on polypropylene and nylon-6 nonwoven fiber mats. The pattern edge is readily visible in reflection, and the average extent of coating under the pattern is observed in transmission.

mm into the nylon-6 for these samples. The extent of diffusion into the open regions between fibers is expected to depend on precursor dose time, the number of ALD cycles, deposition temperature, the compression force, and the structure of the

fiber mat (i.e. nonwoven vs woven). Generally we observe diffusion laterally under the covering mask, but for thicker fiber mat samples, we also observe a vertical diffusion pattern. How dose time, compression and other factors affect the growth pattern will likely depend on substrate chemistry, so we investigate polypropylene and nylon-6 polymer fibers. Results of the patterning studies are shown in Figures 7 through 12. We

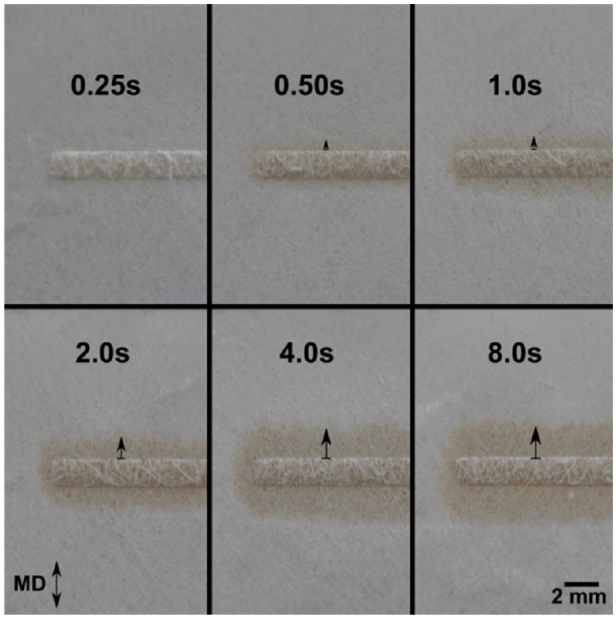

Figure 7. Machine direction cut nylon-6 was patterned with 400 cycles of ZnO ALD using various DEZ dose times. Short dose times produce a feature that is well-defined with minimal diffusion distance beyond the boundary of the compressive mask. Longer dose times result in longer diffusion lengths. This process was repeated for cross direction cut nylon-6 and polypropylene substrates; the results of which are compared and discussed in later sections of this work.

note that while saturated precursor exposure is expected to produce conformal coatings on the fibers, the coating near the growth transition region will likely not be fully conformal. Near the edge of the film growth region, diminished precursor exposure will prevent full surface saturation which is necessary for conformal coverage.

Influence of Precursor Dose Time on Pattern Definition. The effect of DEZ dose time per cycle on precursor diffusion length, and subsequent pattern resolution, is shown in Figure 7 for machine direction cut nylon-6. For these studies, the fibers were "fully" compressed. The shortest dose time of 0.25 seconds per cycle produces a light color, consistent with sub-saturated ALD, whereas dose times of 0.5 seconds and longer lead to darker coating. For dose times exceeding 2 seconds, the coloration extends beyond the masked area, consistent with diffusion into the void space between compressed fibers.

In addition to monitoring lateral film deposition profiles, we can look at vertical growth within relatively thick fiber mats, where only one side of the mat is exposed to precursor. Figure 8 for example, shows a pattern created when 10 fiber mats are stacked and compressed in a pattern before coating in the ALD reaction chamber.

Figure 8a shows photographs: (i) prior to and (ii) after coating with 400 ZnO ALD cycles, where the sample was cut to reveal the vertical penetration pattern. Figure 8b also shows (i) a schematic sample cross section and (ii–iv) a series of nylon-6 nonwoven stacks deposited using different DEZ dose times from 0.5 to 2 seconds. The images (a,ii and b,iv) in Figure 8 correspond to different perspectives of the same sample, showing minimal lateral growth under the mask, but significant vertical growth into the fiber mat stack. The consistent color of the coated region in Figure 8b (images iii and iv) indicates uniform film thickness in the growth zone. The images also show the extent of vertical growth increases with increasing dose time per cycle. Samples can be readily deconstructed layer by layer, to view vertical penetration depth of the precursor. Figure 8c shows the top and bottom three pieces of a ten piece nylon-6 stack.

Number of ZnO ALD Cycles. Growth initiation during ALD is sensitive to the starting surface, especially for deposition on polymer materials.[12,14,17−19] Polypropylene is chemically inert, so ALD nucleation proceeds via sub-surface precursor diffusion. Nylon-6 has amide groups that are more chemically reactive. We measured mass change of polypropylene fiber mats versus number of ZnO ALD cycles and found that nucleation

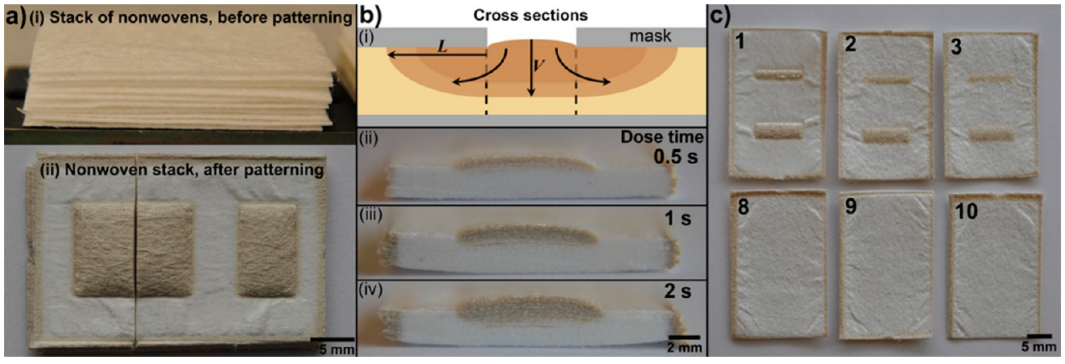

Figure 8. Patterned layers made by compression of porous substrates. Panel a shows a stack of 10 nonwoven nylon-6 mats stacked (i) before and (ii) after compression and patterning. Panel b shows (i) a cross section schematic of precursor diffusing through a sample, where *L* and *V* indicate lateral and vertical diffusion, respectively; and (b,ii-iv) stacks patterned with increasing DEZ dose times. For longer exposure times per ALD cycle, the coating penetrates completely in the vertical direction while maintaining the lateral pattern through the stack. Panel c shows the top three and bottom three layers of a 10 nylon-6 mat tall stack patterned with a 2 second dose time, the numbers signify the position within the stack. The top-most sample (1) is coated uniformly, but the bottom-sample (10) shows minimal coating. ALD can achieve patterned growth with controlled depth on a fiber substrate.

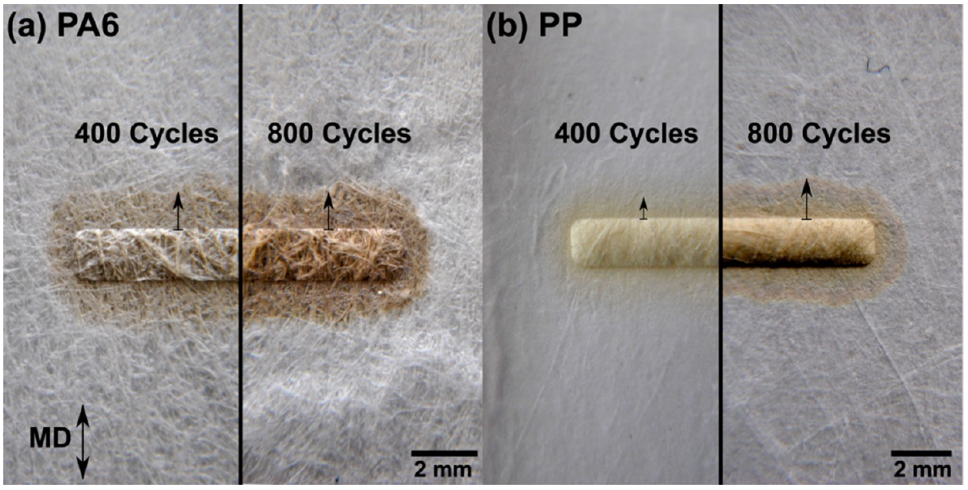

Figure 9. ZnO ALD on (a) nylon-6 nonwoven fiber mats cut in the machine direction and (b) polypropylene nonwoven mats. For deposition on nylon, the extent of diffusion under the masked area is the same for 400 vs 800 ALD cycles, whereas for the polypropylene substrate the 800 cycle deposition is more spread out than the 400 cycle sample. For more deposition cycles, precursor diffusion into the polypropylene polymer may extend growth further under the mask region. The images were digitally enhanced to increase contrast by 50%.

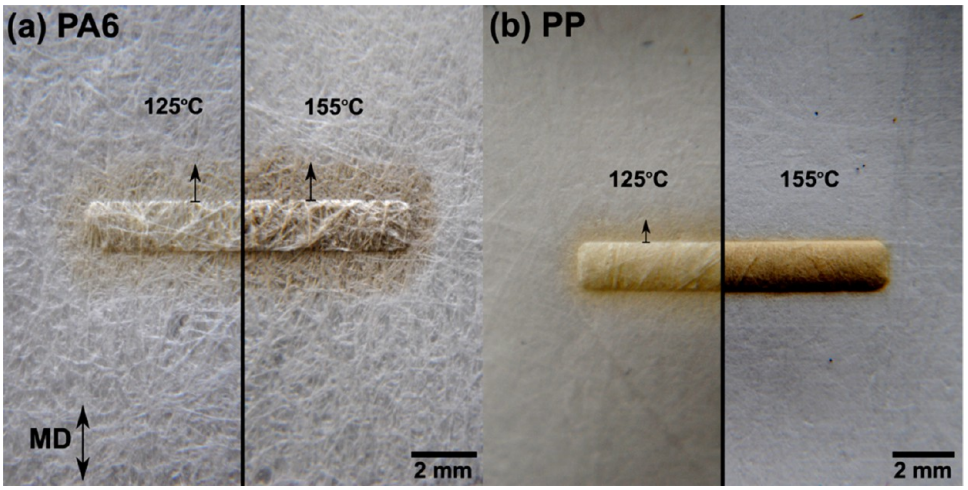

Figure 10. Nonwoven nylon-6 and polypropylene were patterned at 125 and 155 °C to determine the impact of deposition temperature on the pattern. (a) Nylon-6 shows a darker color pattern is created when ZnO is deposited at higher temperature, but the diffusion length, as indicated by the arrows, remains the same. (b) Polypropylene also shows a darker feature when coated at higher temperature, however, the sample also shows significantly lower extent of diffusion of the coating at higher temperatures. Deposition on polypropylene at 155 °C, while under compression may cause the polypropylene to deform, fusing fibers and increasing tortuosity of diffusing precursor molecules. The contrast of the images was increased 50% to make the coated region more apparent.

requires ∼60−90 cycles at 155 °C. After ∼60 cycles, mass increases rapidly then slows to steady growth.[12] On nylon-6 fibers, ZnO mass uptake shows a similar growth incubation period, followed by steady growth. Ellipsometry analysis of film thickness versus cycle number on planar spun cast nylon films further confirms this nucleation trend.

Figure 9 shows images after 400 and 800 ALD cycles for patterned ZnO on (a) nylon-6; and (b) polypropylene substrates. The nylon-6 samples show similar patterns for 400 and 800 cycles of ZnO. The 800 cycle sample appears darker, consistent with a thicker coating layer. The polypropylene substrates, however, show a notably larger growth area after 800 ALD cycles compared to 400 cycles. This may be due to the trends in subsurface versus surface growth for ALD on polypropylene. During the early ALD cycles, before an encapsulating coating is formed, precursor can diffuse into the fibers depleting the gas phase concentration. Subsurface diffusion is blocked after full layer coating, allowing the precursor to reach further into the compressed region as the number of ALD cycles increases.

Deposition Temperature. The deposition temperature is also expected to affect the pattern shape and fidelity. Higher temperatures lead to thermal expansion, followed by melting (at ∼165 °C for polypropylene[12] and ∼215 °C for nylon-6[13]). For conductive coatings, higher deposition temperatures are preferred for higher conductance. Figure 10 shows 400 cycles of ZnO deposited at 125 and 155 °C on MD nylon-6 and polypropylene nonwovens.

On nylon-6, growth under the pattern edge is independent of temperature, whereas on polypropylene the coating is darker (i.e., thicker) and more confined near the feature edge at higher temperature. The more confined growth at higher temperature is ascribed to softening or partial melting of the polypropylene, which will tend to block precursor transport. For further

analysis, the deposition temperature was maintained at 125 °C on polypropylene and 155 °C for nylon-6 substrates.

Extent of Substrate Compression. The extent of fiber compression will influence the distance the precursor travels under the masked region during the dose time. The precursor diffusion coefficient is set by the gas species present in the open spaces (i.e. DEZ in N_2), so we expect any change in precursor travel distance to reflect a change in tortuosity. Figure 11 shows ZnO ALD (400 cycles, 2s DEZ dose/cycle at 155°C on MD nylon-6) patterns on fully and partially compressed nylon-6.

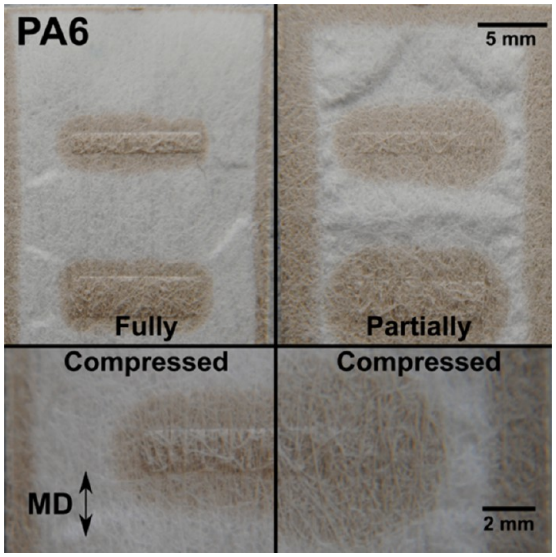

Figure 11. ZnO patterns on nonwoven nylon-6 after coating with 400 cycles at 155 °C. The extent of deposition under the exposed mask depends on the amount of compression used. In this case, "full compression" indicates masking blocks are fully tightened with self tightening screws using a hexagonal wrench, and "partial compression" indicates masking blocks are tightened to finger tight; for consistency, digital calipers were used to measured height of the combined mask and nonwoven samples to verify tightening was consistent throughout a data set.

As expected, the more fully compressed samples show more confined coating for all mats studied. The images for nylon in Figure 11 show the coating is more extended in the machine direction (i.e. along the aligned fibers). For the quantitative analysis discussed below, coating length in the MD and CD are measured and tabulated separately. As noted above, the PP mats have more random fiber alignment, so the extent of coating is independent of direction.

Nonwoven versus Woven Fiber Substrates. To explore the effect of substrate fiber geometry on pattern resolution, we patterned ALD ZnO at 155°C on nonwoven and woven nylon and results are shown in Figure 12.

The images show a much more defined pattern on the nonwoven compared to the woven fibers. The smaller average fiber diameter and random fiber orientation in the nonwoven helps limit lateral reactant transport, thereby enabling better pattern definition.

Coating Distance Under the Mask versus DEZ Dose. Using the optical microscopy images, we quantified the lateral coating distance under the mask edge as a function of the DEZ dose time on polypropylene and nylon-6 nonwovens under full and partial compression, and the resulting data points are plotted in Figure 13. The error bars represent one standard deviation and are shown only for the sample with the largest deviation.

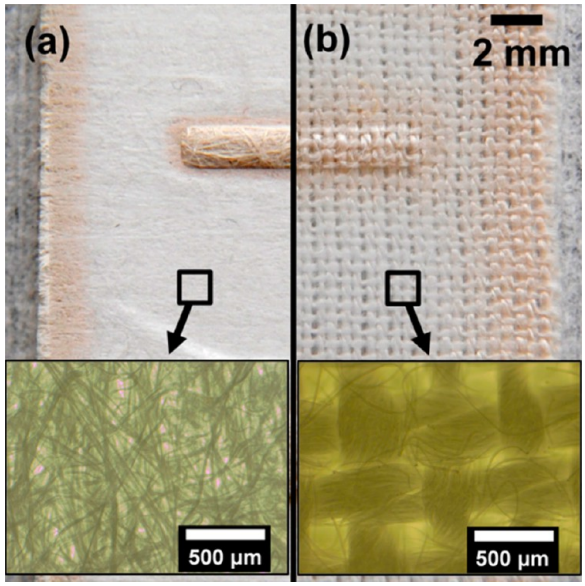

Figure 12. Optical images of (a) nonwoven nylon and (b) woven nylon fiber substrates after pattern-coating with ZnO ALD. Optical microscopy images from each sample show the physical structure of each material. The random orientation of the fibers in the nonwoven compared to the oriented fibers in the woven yarns restricts lateral reactant transport to achieve better feature definition. The images were digitally enhanced to increase contrast by 40%.

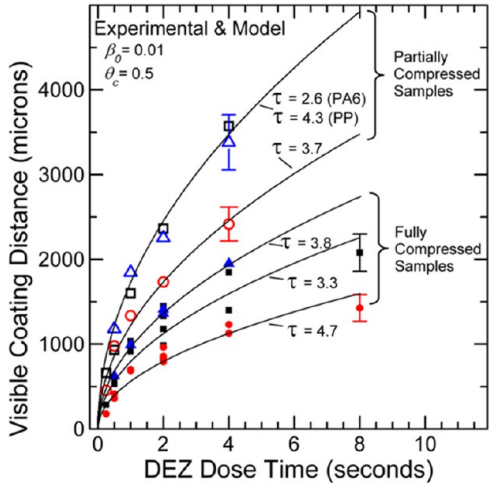

Figure 13. Data from experimental measurements of visible diffusion length for different substrates deposited using various DEZ dose times are shown; polypropylene (blue triangles) and nylon cut in the machine direction (black squares) and cross direction (red circles). Samples were patterned while under both full compression (solid symbols) and partial compression (hollow symbols). Distance measurements were taken using an optical microscope, four micrographs were taken per sample and the maximum and minimum diffusion distances were measured for each. The average distance is plotted, and the error bars shown are for the highest standard deviation sample for each of the data sets. The curves shown are derived from the solutions to eq 4 and 5, which are solved using β_0 = 0.01, θ_C =0.5, each substrates physical parameters ($\overline{S}$, T), but allowing the effective diffusion coefficient (D_{eff}) to vary to fit the data. The tortuosity can then be found for each substrate using eq 6.

As expected, the fiber compression limits the extent of growth under the mask and therefore improves pattern uniformity. We note that if the precursor is not fully consumed during the exposure time, the substrate will continue to be exposed while the precursor moves back out during the purge cycle step. This means that the actual DEZ exposure time may be somewhat larger than the measured DEZ exposure time, especially for the longer exposures. We note that a full model of growth versus cycle number must consider nucleation delay which is present in ZnO ALD on polymers. However, since we find nucleation proceeds similarly on polypropylene and nylon-6, and the data we use for the extent of growth uses a fixed and relatively large number (400) of ALD cycles, the model effectively normalizes the effect of the nucleation delay.

Modeling Reaction-Diffusion for ALD in a Nonwoven. A key aspect for patterning coatings is to understand the mechanisms associated with pattern generation and fidelity. Compressing the fiber mat will reduce reactant transport under the mask edge, but other factors including fiber alignment and ALD process conditions are also found to be important. To understand the interrelations between these parameters, we develop a simple transport model to describe the extent of reactant transport, and analyze how the transport scales as the fiber mats are compressed. We thereby model the extent of growth laterally in the covered or compressed fiber region between the metal masking plates as a function of fiber type, orientation and extent of compression.

The problem geometry is simplified as a 1D semi-infinite media with continuum flow. For some conditions, the Knudsen number is sufficiently large that Knudsen transport could also be considered, but we choose to use continuum molecular diffusion to capture a broad range of process and sample conditions. Specifically, we build on a time dependent reaction-diffusion model described by Yanguas-Gil and Elam[20] for ALD in high aspect ratio materials, but we redefine parameters and introduce terms to better describe ALD in fiber mats. In particular, we redefine specific surface area, $\overline{S}$, in terms of the fiber mats' surface enhancement factor, and we establish an effective diffusion coefficient, D_{eff} to account for the void volume and diffusion tortuosity.

Using conservation of mass and assuming equimolar counter diffusion, the one dimensional unsteady state mass transport follows:

$$\frac{\partial C}{\partial t} = -\frac{\partial}{\partial z}(J_{DEZ}) - r \tag{3}$$

where C is the concentration of DEZ molecules, r is the rate of DEZ loss through chemical reaction, and J_{DEZ} is the precursor flux given by Fick's first law, $J_{DEZ} = -D\ dC/dz$, where D is the diffusion coefficient. The rate of DEZ loss through reaction is determined by the precursor flux to the reactive sites on the wall (J_{wall}), the available surface area (normalized per unit volume) $\overline{S}$, and the surface reaction probability, taken to be first order with respect to available sites (first-order irreversible Langmuir adsorption, $\beta = \beta_0 \cdot \theta$). Equation 3 then becomes[20]

$$\frac{\partial C}{\partial t} = D\frac{\partial^2 C}{\partial z^2} - \beta_0 \cdot \theta \cdot J_{wall} \cdot \overline{S} \tag{4}$$

where β_0 is the initial reaction probability on an un-reacted surface, θ is the fraction of available reaction sites, and $\overline{S}$ is the specific surface area (area per unit volume).

For nonwoven substrates, the value for $\overline{S} = f_{SA}/t_m$ where f_{SA} is the surface area enhancement factor (defined above) and t_m is the thickness of the fiber mat (which decreases upon compression). The values for $\overline{S}$ are ~2500 cm^{-1} for partially compressed polypropylene, ~6800 cm^{-1} for fully compressed polypropylene, ~6200 cm^{-1} for partially compressed nylon-6, to ~12 800 cm^{-1} for fully compressed nylon. By contrast, in a cylindrical pore, $\overline{S} = 2/R$ where R is the pore radius, so this range of $\overline{S}$ values (2000−10 000 cm^{-1}) would be found in pores with R = 2−10 micrometers.

The kinetic theory of gases gives $J_{wall} = 1/4\ C \cdot \overline{v}$ where $\overline{v}$ is the mean thermal speed of the diffusing particles. The rate equation for site consumption during film deposition is given by[20]

$$\frac{d\theta}{dt} = -\frac{1}{4}\overline{v} \cdot C(z, t) \cdot \beta_0 \cdot \theta(z, t) \cdot S_0 \tag{5}$$

where S_0 is the average area of a reaction site.

For growth on a planar surface, $S_0 \approx 20$ Å^2, which corresponds to ~5 adsorbed molecules nm^{-2}.[21] However, on a polymer surface, subsurface precursor diffusion and reaction can be significant.[12−14,19,22] Analysis of the extent of reaction between trimethyl aluminum and various polymers[19] shows an effective adsorption site density (i.e., the effective "number of monolayers" adsorbed per ALD cycle) can be 1000× or more larger than S_0. Therefore, significant subsurface reaction could help limit precursor transport and improve pattern fidelity, although the deposition would not yield a purely metal oxide coating. While studies of DEZ reactions on polymers are not as extensive,[12,18,22] results show that compared to TMA, DEZ leads to much less sub-surface reaction on polyester fibers.[22] For this work using DEZ, therefore, we maintain the value $S_0 \approx$ 20 Å^2.

During the precursor dose time, we set the precursor concentration at the edge of the feature to be constant and vertically uniform. That is, we work under conditions where the vertical transport in the exposed fiber region is fast relative to lateral transport in the covered fibers between the metal plates. The boundary condition at the inlet ($z = 0$) is then, $C(0,t) = C_0$ during the dose time. The value for C_0 was estimated from the measured pressure change upon DEZ dosing, $\Delta P \approx 0.07$ Torr which corresponds to $C_0 \approx 1.6 \times 10^{15}$ molecules cm^{-3}. Far away from the inlet, $C(\infty,t) = 0$. At $t = 0$, $C(z,0) = 0$, and the surface is fully available for deposition: $\theta(z,0)=1$.

The value for β_0 is the probability for reaction between the precursor and available surface site upon collision. For rapid reaction, $\beta_0 = 1$, and a sharp growth boundary will form, while $\beta_0<0.01$ results in a more tapered growth edge profile, but the average coating distance from the edge will not be affected. We use $\beta_0 = 0.01$, but find that under the conditions studied, the outcome is not strongly sensitive to β_0 between 1 and ~10^{-3}.

Equations 4 and 5 are solved using MATLAB for various dose times to determine the expected adsorbed DEZ coverage (i.e., extent of ZnO coating) as a function of normalized distance from the feature edge (z/L). As noted above, the ZnO coating is visible after >100 ALD cycles. After 400 ALD cycles, therefore, the coating edge will appear where the surface coverage per cycle θ is ≥0.25. When β_0 is set between 0.01 and 1 the coating thickness vs. lateral distance into the fiber mat changes abruptly. Therefore, θ between 0.25 and 0.75 produce only a small change (<3%) in the expected visible coating distance. For all samples, we set θ "critical", $\theta_c = 0.5$ in the model to identify the visible coating distance.

Equation 4 also requires input for the diffusion coefficient for DEZ in N_2: D_{DEZ}. This value can be approximated using the value for O_2 diffusion through N_2,[23] adjusted from standard conditions by $D_1 \cdot P_1 \cdot T_1^{-3/2} = D_2 \cdot P_2 \cdot T_2^{-3/2}$. At 155 °C and 1 Torr, this yields $D_{DEZ} \approx 270$ cm^2/s. However, this value for gaseous diffusion needs to be adjusted for diffusion through a porous network[24]

$$D_{eff} = \frac{D_{DEZ} \cdot \varepsilon}{\tau^2} \tag{6}$$

The effective diffusion coefficient, D_{eff}, is less than D_{DEZ} because of the volume void fraction (ε) and the tortuosity within the matrix, τ. The tortuosity is defined as the actual transport path length relative to the linear distance traveled and is generally greater than one

$$\tau = L_{tran}/L_{lin} \tag{7}$$

To calculate the model curves for visible coating distance versus DEZ exposure time, we use parameters defined above for each sample set, that is, f_{SA}, S_0, t_m, and ε, and set $\beta_0 = 0.01$ and $\theta_c = 0.5$, and left the tortuosity, τ as an adjustable parameter. The resulting model curve fits are plotted with the experimental data in Figure 13. The tortuosity, and corresponding D_{eff} values are presented in Table 1.

Table 1. Effective Diffusion Coefficients and Calculated Tortuosity Values for the Model Curves Plotted in Figure 13[a]

		nylon-6		polypropylene	
		tortuosity, τ	D_{eff} (cm^2/s)	tortuosity, τ	D_{eff} (cm^2/s)
partial compression	MD	2.6	30	4.3	11
	CD	3.7	15		
full compression	MD	3.3	13	3.8	9.5
	CD	4.7	6.5		

[a]The effective diffusion coefficients and the tortuosity values calculated under both partial and full compression for both machine direction and cross direction PA6, as well as PP.

For the nylon-6 samples, consistent with expected results, transport is more favorable along the machine direction where fibers are aligned with the precursor diffusion. Moreover, for all samples, we see the effective diffusivity decreases upon compression. However, the tortuosity increases upon compression in the nylon-6, but appears to decrease upon compression in the polypropylene. We interpret these results as follows. In the nylon-6, where fiber alignment is not uniform, compression increases tortuosity and decreases void fraction, leading to a net decrease in D_{eff} and an overall decrease in visible coating distance under the mask. Compared to the nylon-6, the tortuosity is larger in the more random polypropylene. Upon compression the tortuosity in the nylon-6 increases. In polypropylene the apparent decrease in τ is relatively small, and we believe the decrease in travel distance (i.e., the decrease in D_{eff} in Table 1) upon compression is due primarily to a decrease in void fraction (i.e., the small change in τ in compressed polypropylene is not quantitatively significant). It is reasonable that a more random network with smaller fibers (1-5 micrometers for polypropylene versus 5−10 micrometers for nylon-6) will produce a relatively large tortuosity, with relatively small change in tortuosity upon compression.

Overall, the quantitative model describes well the observed trends in pattern extension under the coating mask: larger compression and more random fiber orientation improves the pattern fidelity. The model also suggests that increasing the density of reactive sites in the polymer (i.e., choosing a functionalized polymer and using precursors with more propensity for subsurface diffusion and reaction) will also improve fidelity, but will produce a precursor/polymer fiber mixture rather than a uniform thin film fiber coating.

CONCLUSIONS

A method to pattern and selectively deposit ALD thin film layers on fiber mats was demonstrated using a mask with applied physical compressive force. Patterned ZnO ALD coatings were formed on nylon-6 and polypropylene nonwovens, and we showed how substrate properties such as fiber diameter and orientation, polymer chemistry, and structure (woven vs nonwoven) play a key a role in determining the extent of reactant transport into the covered fiber matrix. Both lateral and vertical penetration of reactive growth species into nonwoven mats was observed, and lateral species transport was modeled to quantitatively analyze the effect of fiber structure and mechanical compression on the extent of coating under the physical mask.

We find that the extent of reactant transport is affected by the amount and direction of fiber alignment within the fiber substrate, and the degree of physical compression applied. By fitting the experimental results for coating distance versus precursor exposure time to a quantitative diffusion model, we find that the mechanisms by which physical compression affects species transport depends on the structure of the starting fiber matrix. For small random fibers, compression predominantly decreases the void volume, whereas for larger and more aligned fibers, compression tends to decrease void volume and increase transport path tortuosity. The quantitative model fits the observed trends in pattern fidelity and provides a valuable tool to estimate the extent of precursor diffusion and transport in fiber matrices during coating by atomic layer deposition.

AUTHOR INFORMATION

Corresponding Author

*E-mail: parsons@ncsu.edu.

Notes

The authors declare no competing financial interest.

ACKNOWLEDGMENTS

We acknowledge the Nonwovens Institute at North Carolina State University (NWI) Project 09-118 for support for W.J.S. We acknowledge Amy Minton for help performing the fiber orientation analysis at the Nonwovens Institute Microscopy and Imaging Lab, Richard Lamy and Christopher Sanford at the NCSU Precision Instrument Machine Shop for help fabricating the patterning masks, and Chuck Mooney at the NC State Analytical Instrument Facility for his assistance with SEM and EDS analysis.

REFERENCES

(1) Campbell, S. A. *Fabrication Engineering at the Micro and Nanoscale*, 3rd ed; Oxford University Press: New York, 2008.

(2) Langston, M. C.; Usui, T.; Prinz, F. B. Mechanical Masking of Films Deposited by Atomic Layer Deposition. *J. Vac. Sci. Technol., A* **2012**, *30*, No. 01A153.

(3) Kodas, T. T.; Hampden-Smith, M. J. *The Chemistry of Metal CVD*, 1st ed.; VCH: Weinheim, Germany, 1994.
(4) Dolan, G. J. Offset Masks for Lift-Off Photoprocessing. *Appl. Phys. Lett.* **1977**, *31*, 337.
(5) Dendooven, J.; Deduytsche, D.; Musschoot, J.; Vanmeirhaeghe, R. L.; Detavernier, C. Modeling the Conformality of Atomic Layer Deposition: The Effect of Sticking Probability. *J. Electrochem. Soc.* **2009**, *156*, 63.
(6) Musschoot, J.; Dendooven, J.; Deduytsche, D.; Haemers, J.; Buyle, G.; Detavernier, C. Conformality of Thermal and Plasma Enhanced Atomic Layer Deposition on a Non-Woven Fibrous Substrate. *Surf. Coat. Technol.* **2012**, *206*, 4511−4517.
(7) Cherenack, K.; van Pieterson, L. Smart Textiles: Challenges and Opportunities. *J. Appl. Phys.* **2012**, *112*, No. 091301.
(8) Wei, Q.; Yu, L.; Wu, N.; Hong, S. Preparation and Characterization of Copper Nanocomposite Textiles. *J. Ind. Text.* **2008**, *37*, 275−283.
(9) Mackus, A. J. M.; Garcia-Alonso, D.; Knoops, H. C. M.; Bol, A. A.; Kessels, W. M. M. Room-Temperature Atomic Layer Deposition of Platinum. *Chem. Mater.* **2013**, *25*, 1769−1774.
(10) Parsons, G. N.; Atanasov, S. E.; Dandley, E. C.; Devine, C. K.; Gong, B.; Jur, J. S.; Lee, K.; Oldham, C. J.; Peng, Q.; Spagnola, J. C.; Williams, P. S. Mechanisms and Reactions During Atomic Layer Deposition on Polymers. *Coord. Chem. Rev.* **2013**, *257*, 3323−3331.
(11) Jur, J. S.; Sweet, W. J.; Oldham, C. J.; Parsons, G. N. Atomic Layer Deposition of Conductive Coatings on Cotton, Paper, and Synthetic Fibers: Conductivity Analysis and Functional Chemical Sensing Using "All-Fiber" Capacitors. *Adv. Funct. Mater.* **2011**, *21*, 1993−2002.
(12) Sweet, W. J.; Jur, J. S.; Parsons, G. N. Bi-Layer Al_2O_3/ZnO Atomic Layer Deposition for Controllable Conductive Coatings on Polypropylene Nonwoven Fiber Mats. *J. Appl. Phys.* **2013**, *113*, No. 194303.
(13) Kalanyan, B.; Oldham, C. J.; Sweet, W. J.; Parsons, G. N. Highly Conductive and Flexible Nylon-6 Nonwoven Fiber Mats Formed using Tungsten Atomic Layer Deposition. *ACS Appl. Mater. Interfaces* **2013**, *5*, 5253−5259.
(14) Spagnola, J. C.; Gong, B.; Arvidson, S. A.; Jur, J. S.; Khan, S. A.; Parsons, G. N. Surface and Sub-Surface Reactions During Low Temperature Aluminium Oxide Atomic Layer Deposition On Fiber-Forming Polymers. *J. Mater. Chem.* **2010**, *20*, 4213.
(15) Guziewicz, E.; Godlewski, M.; Wachnicki, L.; Krajewski, T. A.; Luka, G.; Gieraltowska, S.; Jakiela, R.; Stonert, A.; Lisowski, W.; Krawczyk, M.; Sobczak, J. W.; Jablonski, A. ALD Grown Zinc Oxide with Controllable Electrical Properties. *Semicond. Sci. Technol.* **2012**, *27*, No. 074011.
(16) Mikami, M.; Eto, T.; Wang, J.; Masa, Y.; Isshiki, M. Growth of Zinc Oxide by Chemical Vapor Transport. *J. Cryst. Growth* **2005**, *276*, 389−392.
(17) Wilson, C. A.; Grubbs, R. K.; George, S. M. Nucleation and Growth during Al2O3 Atomic Layer Deposition on Polymers. *Chem. Mater.* **2005**, *17*, 5625−5634.
(18) Oldham, C. J.; Gong, B.; Spagnola, J. C.; Jur, J. S.; Senecal, K. J.; Godfrey, T. A.; Parsons, G. N. Encapsulation and Chemical Resistance of Electrospun Nylon Nanofibers Coated Using Integrated Atomic and Molecular Layer Deposition. *J. Electrochem. Soc.* **2011**, *158*, No. D549.
(19) Gong, B.; Parsons, G. N. Quantitative In Situ Infrared Analysis of Reactions Between Trimethylaluminum and Polymers During Al_2O_3 Atomic Layer Deposition. *J. Mater. Chem.* **2012**, *22*, 15672.
(20) Yanguas-Gil, A.; Elam, J. W. Self-Limited Reaction-Diffusion in Nanostructured Substrates: Surface Coverage Dynamics and Analytic Approximations to ALD Saturation Times. *Chem. Vap. Deposition* **2012**, *18*, 46−52.
(21) Puurunen, R. L. Surface Chemistry of Atomic Layer Deposition: A Case Study for the Trimethylaluminum/Water Process. *J. Appl. Phys.* **2005**, *97*, 52.
(22) Gong, B.; Peng, Q.; Jur, J. S.; Devine, C. K.; Lee, K.; Parsons, G. N. Sequential Vapor Infiltration of Metal Oxides into Sacrificial Polyester Fibers: Shape Replication and Controlled Porosity of Microporous/Mesoporous Oxide Monoliths. *Chem. Mater.* **2011**, *23*, 3476−3485.
(23) Welty, J. R.; Wicks, C. E.; Wilson, R. E.; Rorrer, G. *Fundamentals of Momentum, Heat, and Mass Transfer*, 4th ed; Wiley: New York, NY, 2001.
(24) Epstein, N. On Tortuosity and the Tortuosity Factor in Flow and Diffusion through Porous Media. *Chem. Eng. Sci.* **1989**, *44*, 777−779.